Volume 1 | Number 1 | Jan 2013 | Pages 1–100

Journal of
Materials Chemistry A

Materials for energy and sustainability
www.rsc.org/materialsA

Li⁺

ROYAL SOCIETY
OF CHEMISTRY

ROYAL SOCIETY
OF **CHEMISTRY**

www.rsc.org/materialsA

Journal Name

Dynamic Article Links ▶

ARTICLE TYPE

Core-shell ultramicroporous@microporous carbon nanospheres as advanced supercapacitor electrodes

Mingxian Liu, Jiasheng Qian, Yunhui Zhao, Dazhang Zhu, Lihua Gan* and Longwu Chen

In this paper, we report a novel design and synthesis of core-shell ultramicroporous@microporous carbon nanospheres (UMCNs) for advanced supercapacitor electrodes. Polymer colloids (10–14 nm) are obtained by time-controlled polymerization of phloroglucinol and terephthalaldehyde (P/T). UMCNs with ultramicropores in the inner core and abundant micropores in the outer shell are fabricated by the copolymerization of resorcinol and formaldehyde (R/F) on the surfaces of P/T colloids with the presence of ammonia, followed by
10 carbonization and further KOH activation. As-prepared UMCNs have adjustable diameter (52–74 nm) and high specific surface area (up to 2156 m^2 g^{-1}). Inter-particle mesoporosity among UMCNs creates ion buffer reservoirs and reduces ion diffusion distance, while micropores offer highly efficient ion channels and also show high capability for charge accumulation. Moreover, regular ultramicropores benefit the fast transportation and diffusion of electrolyte ions. Consequently, UMCNs with unique 3D core-shell nanostructure exhibit superb electrochemical performance such as very high specific capacitance (411 F g^{-1} at 1 A g^{-1}), ultra-high rate capability (charge–
15 discharge operation under an extremely high current density of 100 A g^{-1}), excellent long-term cycle stability (10000 cycles) and reasonable energy density at high power density (5.94 W h kg^{-1} at 50 kW kg^{-1}) in 6 M KOH electrolyte. This finding opens up a new window for well-developed carbon nanoarchitectures to support advanced supercapacitor devices for high rate electrochemical energy storage.

Introduction

20 The global economy and ecology have been seriously affected by climate change and energy shortage of fossil fuels,[1] putting great obstacles in the way of building a better society. Therefore, there has been an ever increasing interest and urgent requirement for highly efficient, clean and sustainable power resources, as well as
25 advanced energy storage and conversion technologies, such as lithium-ion batteries and supercapacitors.[2–6] Supercapacitors, also known as ultracapacitors or electrochemical capacitors, have attracted extensive attention in a wide range of applications such as mobile electronic devices, pure and hybrid electric vehicles,
30 and other renewable energy storage systems due to high power density, fast charge–discharge process and long cycle life.[1, 7–12] Based on the energy storage mechanism, supercapacitors can be classified into electric double-layer capacitors (EDLCs) and faradaic pseudo-capacitors.[13, 14] Electrostatic storage of electrical
35 energy in EDLCs is achieved by the accumulation of ionic charges occurred in the double-layer at electrode/electrolyte interface;[15] accordingly high specific surface area coupled with fast ion transport channel is required for the rapid formation of a double-layer.[16]
40 Microporous carbons (*e.g.* activated carbons) are one of the most used electrode materials for EDLCs.[17–19] They show high capability for electrostatic charge accumulation at the interface of electrode/electrolyte due to large surface area, and thus contribute to high electrochemical capacitance and energy density of EDLCs.
45 However, the island-like and irregular micropores in most of these materials often prevent or slow down the ion transport, and thus cause much difficult to construct a high-power density EDLC.[18] By contrast, ordered mesoporous carbons exhibit much better rate performance because larger and well structured
50 mesopores allow electrolyte ions to transfer rapidly during the charge–discharge process, especially at high current density.[21-23] Unfortunately, larger mesopores is usually in contradiction with high surface area, leading to insufficient specific capacitance and relatively low energy density of the final EDLC devices.
55 Therefore, an optimum pore size is supposed to two seemingly contradictory requirements: as small as possible for high surface area to ensure high energy density, but as large as possible for rapid ion transportation to achieve high power density.[16, 24]

In principle, it has been demonstrated that micropores larger
60 than 0.5 nm are accessible electrochemically for aqueous ions.[24, 25] Therefore, microporous carbons can be used in a better way in EDLC electrodes when the disordered micropores are properly optimized for finally reaching the point where both high surface area and fast and efficient ion diffusion pathway become a reality.
65 [16, 25–28] For example, zeolite-templated ordered microporous carbons with high surface areas (3040 m^2 g^{-1}) and regularly arrayed and three-dimensionally-linked pores (1.2 nm) exhibits high gravimetric capacitance (140–190 F g^{-1}) in an organic electrolyte solution, and such a high capacitance can be well
70 retained even at a very high current density up to 20 A g^{-1}.[16] Poly(vinylidene fluoride)-derived ultramicroporous carbons with a surface area of 1012 m^2 g^{-1} and a regular pore size of 0.55 nm show an electrochemical capacitance of 264 F g^{-1} in 6 M KOH electrolyte.[24] Chmiola et al. discovered that pore size less than 1
75 nm show an anomalous contribution in capacitance of EDLCs.[29–31] Therefore, high-surface-area regular ultramicroporous carbons

Journal of Materials Chemistry A Accepted Manuscript

can be considered as a good choice for EDLC electrodes.

Carbon spheres which take the advantages of regular geometry, adjustable and controllable diameter and porosity over carbon powders, monoliths or flakes are innovative materials for use in photonic crystals, adsorption, catalysis, energy storage, controlled drug delivery, etc.[32–37] Therefore, many efforts were focused on the synthesis and application of micro- or nanometer sized carbon spheres during the past several years.[38–45] For example, Liu et al. extended the classic Stöber method to prepare submicrometer-scaled resorcinol/formaldehyde polymer and carbon spheres with highly uniform and controllable diameter.[40] The Stöber method also provides new opportunities for the synthesis of micro- and/or mesoporous carbon spheres.[41] Based on benzoxazine chemistry, the Lu group achieved the precise control over the diameters of carbon nanospheres using a temperature-programmed method.[42] Homogeneous package among carbon spheres creates inter-particle porosity which promotes the formation of ion buffer reservoirs, reducing the transportation distance of electrolyte ions to the interior carbon surfaces. Consequently, porous carbon spheres are emerging as powerful electrode materials for EDLCs due to the decreased resistance of ion diffusion. [9, 32–34, 36–39, 46]

Taking into account all the aspects mentioned above, carbon materials combined high surface area, regular ultramicropore and spherical geometry simultaneously would represent promising and innovative materials and are expected to be particularly suitable for high performance EDLCs. To aim that target, we herein demonstrate the development of novel 3D core-shell ultramicroporous@microporous carbon nanospheres (UMCNs) as advanced electrodes for ultra-high rate electrochemical energy storage. By time-controlled polymerization of phloroglucinol and terephthalaldehyde (P/T), polymer colloids are prepared, and then resorcinol/formaldehyde (R/F) copolymerizes on the colloid surfaces to fabricate P/T@R/F nanospheres. Carbonization and further KOH activation generates regular ultramicropores in the inner P/T cores and abundant micropores in the outer R/F shells. The resultant UMCNs with unique nanoarchitecture exhibit very high gravimetric capacitance, ultra-high rate capability, excellent long-term cycle life and high power density. The methodology presented in this work highlights promising prospects of the well-designed carbon materials for advanced supercapacitor devices.

Experimental

Materials

Phloroglncinol, terephthalaldehyde, ammonia solution (25 wt%), resorcinol, formaldehyde solution (37–40 wt%), and KOH were analytical reagents purchased from Sinopharm Chemical Reagent Co., Ltd. Polytetrafluoroethylene (PTFE, catalog no. FR301B) was purchased from Shanghai 3F New Materials Co., Ltd. Nickel foam was purchased from Shanghai Hongxiang Plant. Pure nitrogen was supplied by Shanghai BOC Special Gases Sales Service Co., Ltd. All chemicals were used as received without further purification.

Synthesis of core-shell UMCNs

0.063 g (0.5 mmol) of phloroglncinol, 0.05 g (0.375 mmol) of terephthalaldehyde and 28 mL distilled water was mixed and stirred at 70 °C for 30–120 min to prepare P/T polymer colloid sol (denoted as P/T-x, hereinafter x represents the reaction time). 0.165 g (1.5 mmol) of resorcinol was added into the sol under stirring for 30 min. After that, 0.1 mL ammonia and 0.225 mL formaldehyde solution (3.0 mmol) was added to the above system and stirred for 24 h at 25 °C, followed by heating at 100 °C in a Teflon-lined autoclave for 24 h to fabricate P/T@R/F polymer nanospheres. The nanospheres were centrifuged and dried at 100 °C, followed by carbonization at 850 °C (5 °C min^{-1}) for 4 h under N_2 flow to prepare ultramicroporous carbon nanospheres (UCNs, denoted as UCN-x). The UCNs were further chemically activated by KOH (UCNs/KOH=1:3, w/w) at 800 °C for 2 h in a nitrogen atmosphere to fabricate core-shell UMCNs (denoted as UMCN-x).

Characterization

Scanning electron microscopy (SEM) observation was done on a Hitachi S-4800 equipment. Transmission electron microscopy (TEM) characterization was conducted using a JEM-2100 instrument operated at 200 kV. Before TEM observation, the sample was dispersed in ethanol, and the suspension was dropped on a carbon-coated copper grid. Dynamic light scattering (DLS) test was carried out at 25 °C on a Malvern Zetasizer ZEN 3690 instrument. Nitrogen adsorption and desorption analysis was taken on Micromeritics ASAP 2020 porosimeter. The specific surface area was calculated by Brunauer–Emmett–Teller (BET) method. Nonlocal density functional theory (NLDFT), the cylindrical model, was utilized to obtain the pore size distribution.

Electrochemical measurement

Electrochemical measurements were performed in a two electrode cell (capacitor) with 6.0 M KOH electrolyte solution. For the preparation of one electrode, 90 wt% active material was mixed with 10 wt% PTFE binder (PTFE 60 wt% dispersion in ethanol) to form slurry. The slurry was spread onto a nickel-foam (1 cm^2) under 25 MPa, followed by drying at 100 °C to prepare an electrode (1.0 mm thick, ~10 mg). After that, two electrodes with same weight were put together, and then a polypropylene membrane was sandwiched between them as a separator. Two identical electrodes were used as cathode and anode for the cell configuration. The capacitor cell was pumped for 30 min before measurement so that the active material was soaked fully by the electrolyte. Cyclic voltammetry (CV) and galvanostatic charge–discharge (GCD) measurements were carried out on a CHI 660D electrochemical workstation with a potential window of 0–1.0 V. Electrochemical impedance spectroscopy (EIS) (frequency range between 1 mHz and 10^3 kHz) was conducted on the CHI660D system. The gravimetric capacitance (C, F g^{-1}) was calculated from CV curves using equ (1).

$$C = \frac{\Delta Q}{2 \times \Delta V \times m \times r} \tag{1}$$

In which ΔQ is the charge integrated from the voltage range, ΔV is the voltage window, m is the mass of carbon on two electrodes, r is the scan rate. The specific capacitances of the electrodes were also calculated from GCD datum using equ (2).

$$C = \frac{I \times \Delta t}{\Delta V \times m} \tag{2}$$

Where I is the discharge current, Δt is the discharge time, ΔV is the voltage difference within the discharge time Δt, and m is the total mass of carbon on two electrodes. The energy density (E, W h kg^{-1}) and power density (P, kW kg^{-1}) were calculated from equ (3) and (4).

$$E = CV^2 / 2 \tag{3}$$

$$P = IV / 2 \tag{4}$$

Here C, V, I is gravimetric capacitance, the cell voltage and the current density.

Results and discussion

Due to the electron donating resonance effect of the three hydroxyl groups (–OH), phloroglucinol is highly reactive towards electrophilic aromatic substitution such as formaldehyde or terephthalaldehyde.[47–50] P/T could polymerize through a process that the carbonyl group in terephthalaldehyde is attacked by the electron-rich phenyl rings and links with two phloroglucinol molecules by the elimination of a water molecule.[47] Fig. 1 shows a typical TEM image and DLS data of P/T-60 polymer colloids. These colloids have a mean size of ~12 nm. Time-controlled P/T polymerization results in the formation of polymer colloids with tunable diameters. Longer reaction time leads to bigger P/T polymer colloids, as shown in the inset of Fig.1b. When increase the polymerization time from 30 to 120 min, the mean sizes of the polymer colloids increase from about 10 to 14 nm.
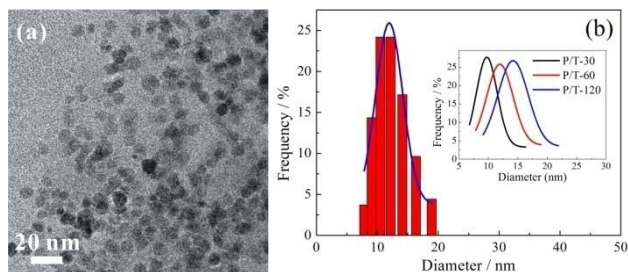

Fig. 1 A typical TEM image (a) and DLS data (b) of P/T-60 polymer colloids (The inset shows fitted curves of DLS data of P/T-30, P/T-60 and P/T-120).

　　Fig.2 gives representative SEM and TEM images of UMCN-60. As-prepared carbon nanospheres have uniform spherical morphology in large domains (Fig.2a-b). The sizes of UMCN-60 range from about 40 to 100 nm with an average diameter of ~62 nm, as shown in Fig.2c. The mean diameters of the polymer colloids increase from about 10 to 14 nm (Fig.1b) when increase the P/T polymerization time from 30 to 120 min, and the average diameter of the UMCNs decrease from 74 to 52 nm obtained by DLS data, as shown in the inset of Fig.2c. During the preparation process, emulsion droplets were formed through the H-bonding of water, alcohol and R/F with the presence of ammonia.[40] Colloids can stabilize emulsion droplets, prevent agglomeration and thus reduce the droplet sizes. As a result, longer reaction time encourages the formation of smaller polymer and carbon spheres.
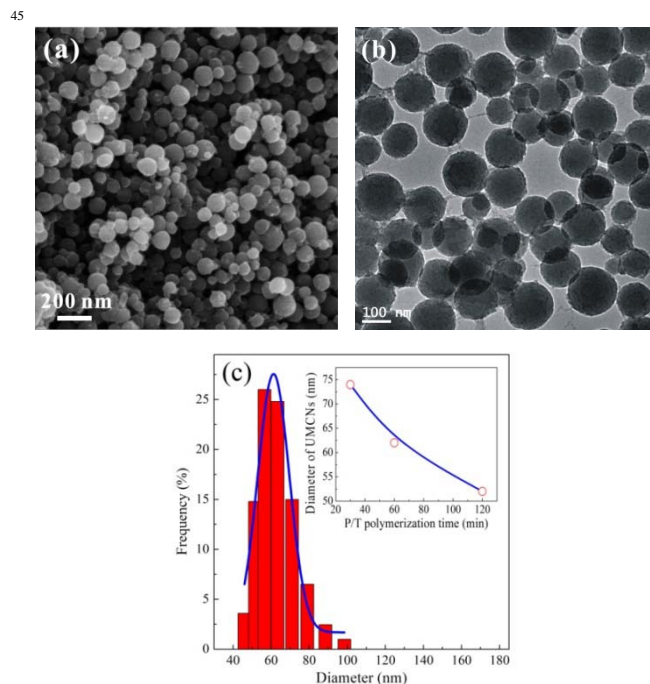

Fig. 2 SEM (a), TEM (b) images of UMCN-60 and DLS data (c) of UMCNs (The inset shows the relationship between the mean diameters of UMCNs and P/T polymerization time).

　　Fig. 3a shows N_2 adsorption and desorption isotherms of UCN-60 and UMCN-60. Thee isotherms belong to type I curve ($P/P_0 < 0.9$), according to the classification of the International Union of Pure and Applied Chemistry.[51] The steep increase in the adsorbed volume at a very low relative pressure ($P/P_0 < 0.05$) is given by microporous solids.[27] Besides, a N_2 condensation step with a very week hysteresis loop is observed in the isotherms at a relative pressure $P/P_0 > 0.9$, indicating the presence of mesoporosity. UCNs shows regular ultramicropores centered at ~0.6 nm, and other weak pore size distributions, as shown in Fig.3b. The ~0.6 nm ultramicropores is a characteristic of P/T derived carbons, [27, 47, 50] and a small quantity of other micropores of UCNs can be ascribed to the R/F polymer decomposition during high temperature carbonization. The mesopores correspond to the interparticle cavities resulted from the stacking of carbon nanospheres. Generally, only carbonization process could not generate those regular ultramicropores in R/F polymer-derived carbons. Therefore, the above result indicates that there are regular ultramicropores in the cores and some micropores in the shells of UCNs. UCNs show similar specific surface areas of 391 (UCN-30), 447 (UCN-60) and 472 m^2 g^{-1} (UCN-120). The ultramicro-, micro-, and mesopores of UMCNs were enhanced by KOH chemical activation (Fig.3b). Carbonization results in regular ultramicropores of ~0.6 nm in the inner cores and few micropores in the outer shell of UCNs, while further KOH activation generates enhanced micropores for the shell layer of UMCNs. Consequently, the surface areas of UMCNs were significantly increased to 1128 (UMCN-120), 1692 (UMCN-30) and 2156 m^2 g^{-1} (UMCN-60). Besides, UMCN-60 has the highest surface area, which could be ascribed to their suitable diameter. The P/T core shows no obvious difference in size, but UMCN-30

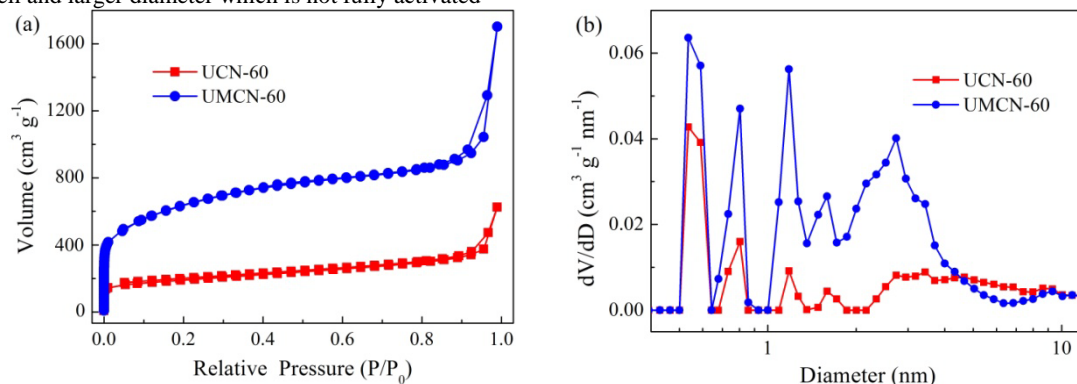has thicker shell and larger diameter which is not fully activated

Fig. 3 Nitrogen absorption–desorption isotherms (a) and pore size distributions curve (b) of UCN-60 and UMCN-60.
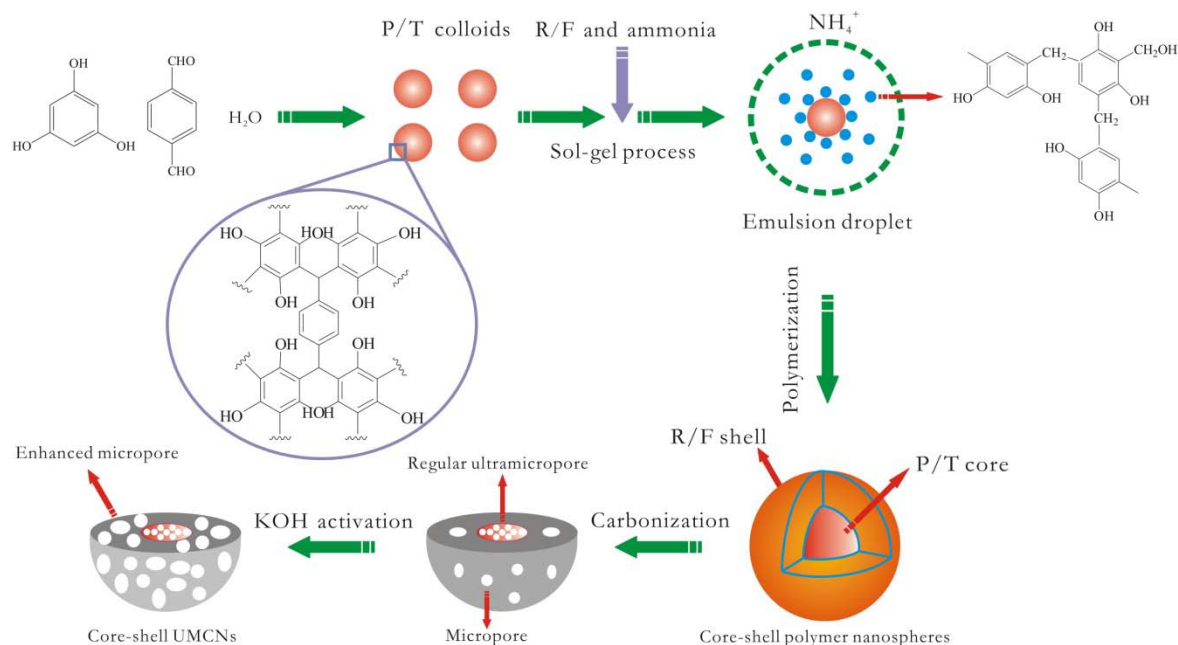

Fig.4 Schematic synthesis of 3D core-shell UMCNs with regular ultramicropores in the cores and abundant micropores in the shells.

by KOH, while UMCN-120 has thinner wall and smaller size, leading to over reaction of KOH with carbons.

Fig.4 shows the schematic synthetic process of the 3D core-shell UMCNs. Time-controlled polymerization of P/T makes the formation of polymer colloids with tunable mean sizes of 10–14 nm (Fig.1b). Then, R/F was polymerized on the colloid surfaces to obtain P/T@R/F polymer nanospheres by using extended Stöber method with the presence of ammonia.[40] In the reaction system, emulsion droplets were formed through the hydrogen bonding of water, alcohol and R/F. There are hydroxyl groups on the surface of P/T polymer colloids which can form stable H-bonds with R/F. Therefore, the polymerization of R/F limited in the inside of emulsion droplets and on the surface of P/T colloids generate core-shell polymer nanospheres. P/T colloids have a mean size of 10–14 nm (Fig.1b), and the resultant UMCNs show the average diameter of 52–74 nm (Fig.2c), suggesting the encapsulation of P/T colloids within R/F polymer shell. In other words, P/T colloids serve as cores, and R/F reacts on the core surfaces to assemble unique P/T@R/F nanospheres. On the other

hand, UCNs exhibit regular ultramicropores centered at ~0.6 nm, and the ultramicro-, and micropores of UMCNs were enlarged after KOH activation (Fig. 3b). This result indicates that UMCNs have a core-shell structure with regular ultramicropores in the inner P/T cores and abundant micropores in the outer R/F shells.

CV curves of UCN electrodes were shown in Fig. 5a. The electrodes exhibit quasi-rectangular shapes at a scan rate of 100 mV s^{-1} in the whole potential window. The UCN packing can generate inter-sphere mesoporous voids which offer high transfer rate of electrolyte ions.[52] UCN-60 electrode shows a specific capacitance of 85 F g^{-1}, larger than that of UCN-30 (60 F g^{-1}) and UCN-120 electrode (54 F g^{-1}) due to higher surface area. Fig. 5b gives CV curves of UCN-60 electrode at scan rates between 200 and 1000 mV s^{-1}. These curves are distorted with increasing scan rate, which can be ascribed to the limited ion incorporation into the active materials.[53] Fig. 5c shows GCD curves of UCN electrodes at 1.0 A g^{-1}. Basically, they are linear and symmetric, but show voltage drop at the beginning of discharge process, suggesting relatively large internal resistance. UCN-60 electrode
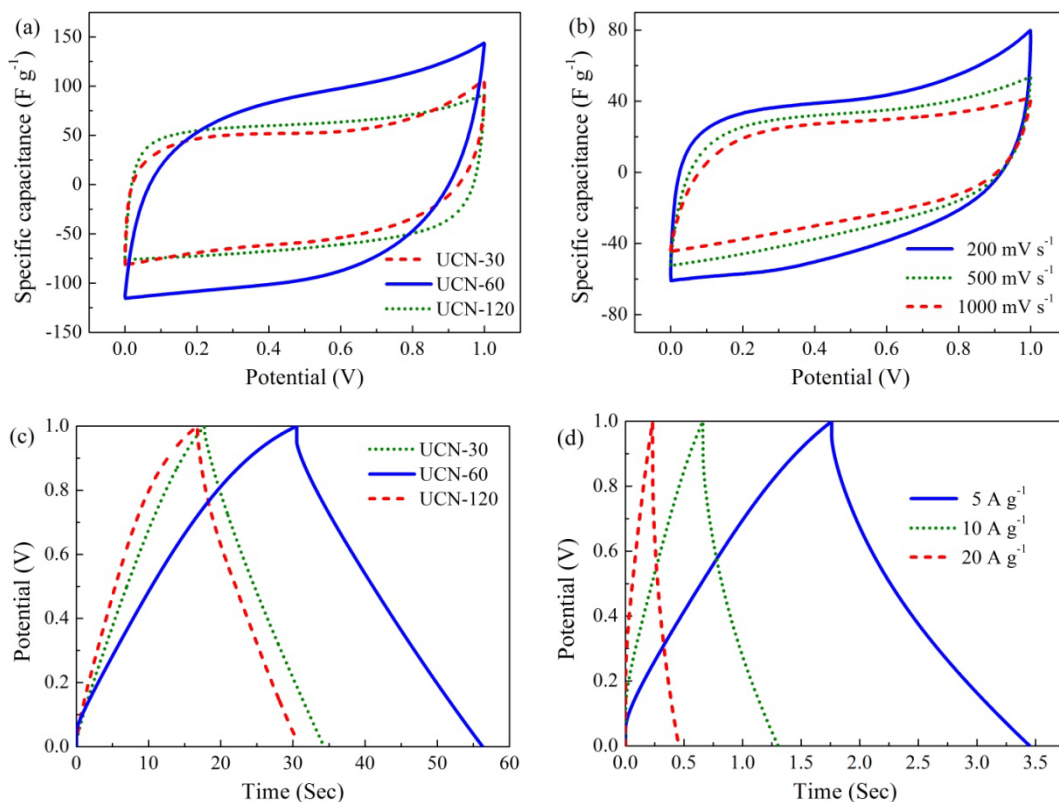
Fig. 5 CV curves of UCN electrodes at 100 mV s^{-1} (a), CV curves of UCN-60 electrode at various scan rates (b), GCD curves of UCN electrodes at 1.0 A g^{-1} (c) and GCD curves of UCN-60 electrode CV at different current densities (d) in 6 M KOH electrolyte solution.
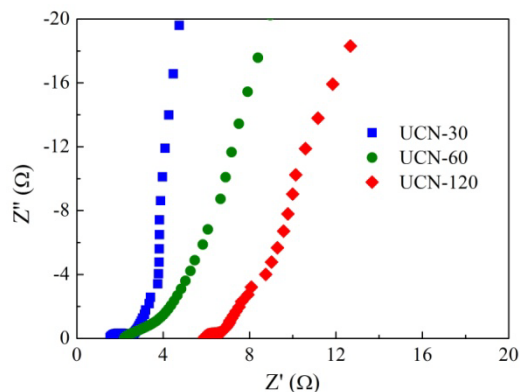

Fig.6 Nyquist plots of UCN electrodes in 6 M KOH solution.

shows an electrochemical capacitance of 115 F g^{-1} at 1.0 A g^{-1}, higher than that of UCN-30 (74 F g^{-1}) and UCN-120 electrode (66 F g^{-1}). Fig. 5d shows GCD curves of UCN-60 electrode at current densities of 5, 10 and 20 A g^{-1}. The potential−time profiles still maintain a triangular shape. However, the specific capacitance of UCN-60 electrode is 83 F g^{-1} at 10 A g^{-1}, lower than those of ultra-, or microporous carbons.[16, 24, 27] The core of UCNs has regular ultramicropores which can be available for aqueous electrolyte ions, but there are not enough micropores in shell layer for ion transportation into the inner electrochemically active surface. That is, only the outer surface or subsurface of UCN electrodes is utilized for charge storage.

EIS analysis was conducted to understand the conductive and diffusive behavior of UCN electrodes. Fig. 6 shows the Nyquist plots of UCN electrodes in 6 M KOH electrolyte solution. The existence of an almost vertical line at low frequency implies good electrochemical capacitive properties of UCN electrodes. A near 45° straight line at the intermediate frequency denotes the feature of ion diffusion or transportation resistance into the electrode. At the high frequency, the presence of the semicircle corresponds to polarization resistance or charge transfer resistance of electrode. The first intersection point on the Z′ axis reveals the equivalent series resistance (ESR), which comprises electrolyte resistance, the intrinsic resistance of the active material, and the interfacial contact resistance of the active material/current collector.[6, 27, 54] The ESR values of UCN-30, UCN-60 and UCN-120 electrodes are 1.5, 2.2 and 5.9 Ω, respectively, much higher than those of our previous reported carbons,[9] which could be ascribed to the limited ion transport due to the lack of pore channels in the shell of the carbon nanospheres. Therefore, further KOH activation of UCNs to generate enhanced micropores for highly efficient transportation of electrolyte ions into the ultramicroporous cores would definitely improve the electrochemical performance.

As expected, CV curves of UMCN electrodes shown in Fig. 7a exhibit good rectangular-like shape at a high scan rate of 1.0 V s^{-1}. Moreover, UMCN-60 electrode still retains a rectangular-like shape even at an extremely high scan rate of 5 V s^{-1} (Fig. 7b), which means fast ion-transport into the inner electrochemically active surface and excellent capacitive behavior of the electrode in quick charge–discharge operations. Fig.7c shows the relationship between the electrochemical capacitances of UMCN
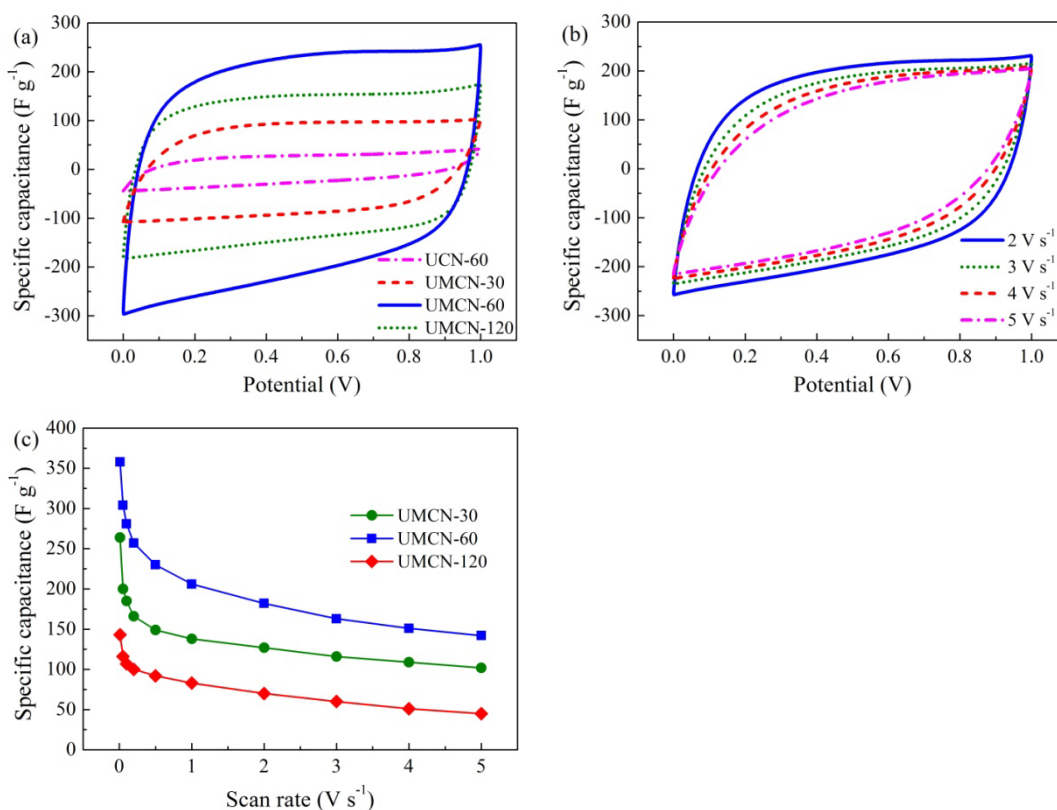
Fig. 7 CV curves of UCN and UMCN electrodes at a scan rate of 1000 mV s^{-1} (a), CV curves of the UCN-60 electrode at various scan
5 rates (b), and the relationship between the specific capacitances of UMCN electrodes and the scan rates (c).

electrodes and the scan rates. Due to the largest surface area,
UMCN-60 electrode shows the highest gravimetric capacitances
which are 358 and 281 F g^{-1} at a scan rate of 10 and 100 mV s^{-1}.
The latter is about 3.3 times more than that of UCN-60 electrode
10 (85 F g^{-1}) under the same scan rate. Besides, UMCN-60 electrode
still retains 206 F g^{-1} at 1 V s^{-1} and 143 F g^{-1} at an extremely
high scan rate of 5 V s^{-1}, far beyond most pure carbon-based
materials. The excellent electrochemical performance of UMCN
electrodes can be ascribed to four aspects: (a) the package
15 mesoporosity among carbon nanospheres serves as ion buffer
reservoirs and reduces the transportation distance of electrolyte
ions to the interior carbon cores,[52] (b) KOH generated-micropores
on the outer shell layer provide sufficient and highly efficient
channels for the diffusion of ions into the inner core layer, (c)
20 regular ultramicropores on the cores benefit fast transportation
and diffusion of electrolyte ions, and (d) large surface area offer
plentiful adsorbing sites for ions and show high capability for
charge accumulation at the electrode/electrolyte interface, and
thus strengthen the electric double-layer capacitance.
25 Fig. 8a shows GCD curves of UMCN electrodes at a high
current density of 10 A g^{-1}. These curves exhibit regularly
triangular shapes with good symmetry at the whole potential
window of 0–1.0 V, suggesting high coulombic efficiency and
good reversibility. Moreover, the potential–time profile of
30 UMCN-60 electrode still maintain a triangular shape even at an
extremely high current density of 100 A g^{-1} (Fig.8b), implying
that the electrode is especially suitable for application in
advanced supercapacitors where rapid charge–discharge is

required. There are no apparent Ohmic drops during the discharge
35 process, corresponding to excellent electronic conductivity and
low ESR.[55] The ESR values for UMCN-30, UMCN-60 and
UMCN-120 electrodes are 0.28, 0.33 and 0.82 Ω, respectively,
which much lower than those of UCNs, as shown in Fig.8c.
Besides, compared with the semicircles existed at the high
40 frequency in UCN electrodes (Fig.6), no such semicircles were
observed for the UMCN samples indicating good charge transfer
of the working electrodes.[56] Fig.8d gives the specific capacitances
of UMCN electrodes under different loading current densities.
UMCN-60 electrode shows an exceptional specific capacitance as
45 high as 411 F g^{-1} at a current density of 1.0 A g^{-1}, much higher
than those of UMCN-60 (312 F g^{-1}), UMCN-60 (141 F g^{-1}) and
UCN-60 electrode (115 F g^{-1}) under the same current density. A
comparison of our electrode with other pure carbon-based
electrodes reported in the literatures is summarized in Table 1.
50 UMCN-60 electrode has advantage over most carbon-based
materials (and carbon/carbon composites) such as microporous
carbons (*e.g.* ordered microporous carbons,[16] activated carbon
monolith,[17] ultramicroporous carbons, and MOF-derived
nanoporous carbons[57, 58]), mesoporous carbons (*e.g.* mesoporous
55 carbon nanofibers,[23] KOH-activated ordered mesoporous
carbons,[59] mesoporous carbon thin film[60] and mesoporous carbon
spheres[9, 33, 61]), hierarchical porous carbons,[62, 63] carbon nanotubes
(*e.g.* carbon nanotube balls,[64] and carbon nanotubes/hollow
carbon spheres[65]), graphene (*e.g.* carbon spheres/graphene
60 nanosheets,[34] graphene nanosheets,[66] graphene nanofibers,[67] and
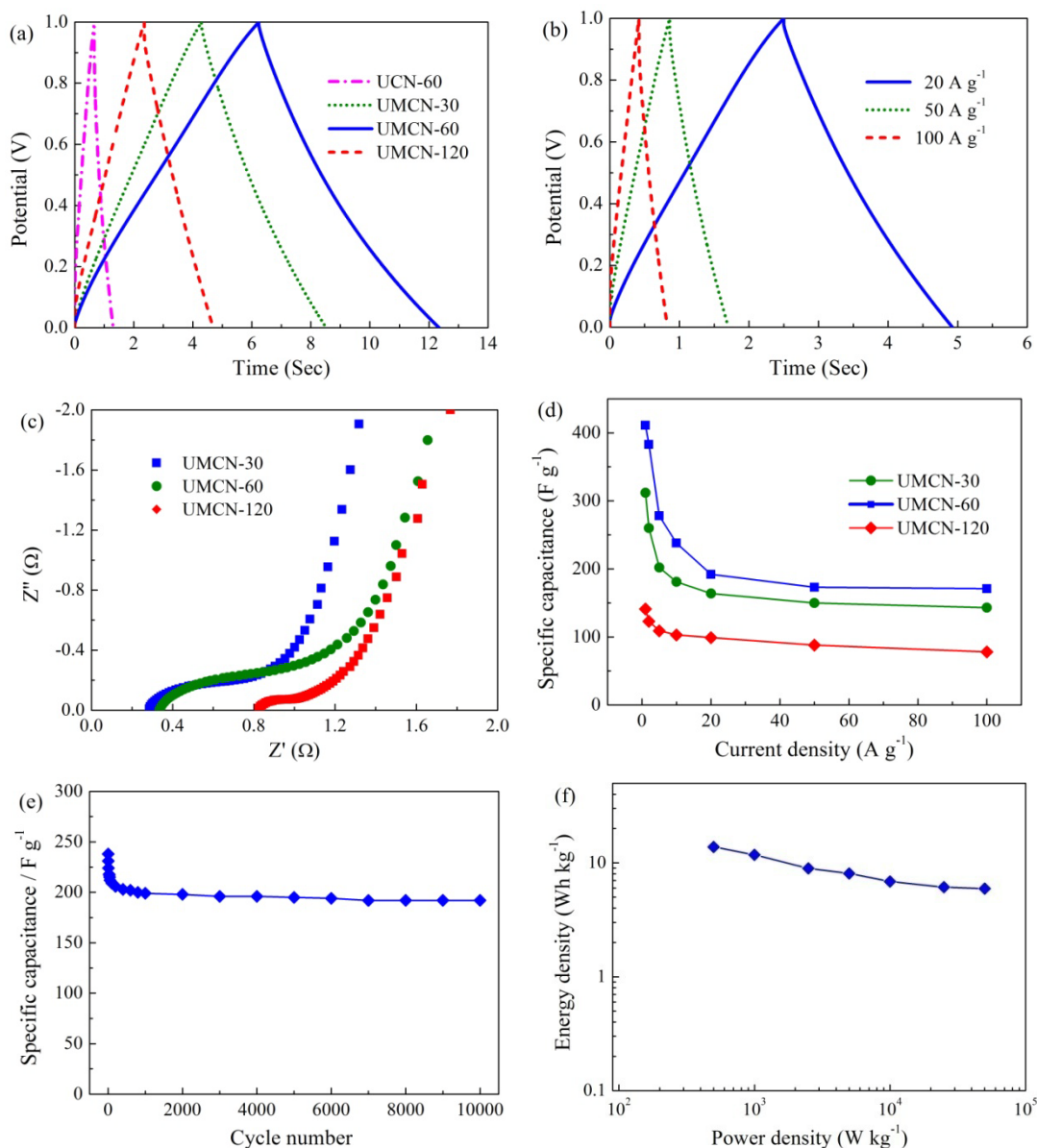activated graphene[68]), and carbon nanocage,[54] and carbon

Fig. 8 GCD curves of UCN and UMCN electrodes at 10 A g^{-1} (a), GCD curves of UCN-60 electrode CV at various current densities (b), Nyquist plots of UCN electrodes (c), the relationship between the specific capacitances of UMCN electrodes and the scan rates (d), Long-term cycle stability of UMCN-60 electrode at 10 A g^{-1} (e), and Ragone plots of the UMCN-60 based asymmetric capacitor (f).

nanoscale networks,[69] etc. At a high current density of 10 A g^{-1}, UMCN-60 electrode also shows a higher gravimetric capacitance compared with the above-mentioned carbons or carbon/carbon composites. Furthermore, the electrode still retains a capacitance of 192 F g^{-1} at 20 A g^{-1} and 170 F g^{-1} even at an extremely high current density of 100 A g^{-1}, exhibiting superb high-rate charge–discharge characteristics.

Long cycle life is an important parameter during the practical applications of an electrode material for energy storage devices. To evaluate the cycle stability of UMCN-60 electrode, a loading current density of 10 A g^{-1} was taken to characterize the long-term charge–discharge behavior, as shown in Fig.8e. UMCN-60 electrode retains 199 F g^{-1} during the first 1000 cycles, 83.6% retention of the original capacity (238 F g^{-1}). After that, the specific capacitance of UMCN-60 electrode only drops 7 F g^{-1} from 199 to 192 F g^{-1} up to 10000 cycles, suggesting a superior electrochemical cycling stability. Generally, carbon-based electrode materials have a long cycle life but suffer from low specific capacitance.[70] The unique structural advantage of our core-shell ultramicroporous@microporous architecture endows excellent cycle stability coupled with high specific capacitance, which provides great potential for widespread supercapacitor application. Fig.8f shows Ragone plots of the asymmetric capacitor determined using the two-electrode full cell configuration. This device shows a high specific energy of 13.78 W h kg^{-1} at a specific power of 500 W kg^{-1} under a current density of 1.0 A g^{-1}. The specific power increases to 50 kW kg^{-1}, maintaining the specific energy of 5.94 W h kg^{-1} at 100 A g^{-1}.

Table 1. A comparison of our electrode data with other pure carbon-based materials reported in the literatures.

Materials		Specific capacitance (F g⁻¹) (measured in aqueous electrolyte)				Ref.
		0.5 A g⁻¹	1.0 A g⁻¹	10 A g⁻¹	20 A g⁻¹	
Microporous carbon	UMCN-60	-	411	238	192	Present work
	NPC₆₅₀	188	-	-	-	57
	ZTC	-	190	-	-	16
	PVFC	218	194	133	-	24
	C1000	~200	-	-	-	58
Mesoporous carbon	FDU-15	130	119	100	-	59
	Thin film	136	-	85*	-	60
	MCM-70-5.5	-	268	-	163	9
	MC-1	208		~170		61
	Nanofibers	280	-	200*	-	23
Hierarchical porous carbon	HPCFs	-	206	182	-	62
	HPGC	~200	~190	~170	~160	63
Carbon nanotube	CNT	-	80	~50	-	64
	CNT-HCS	201.5	~180	~140	139	65
Graphene	GNS	-	252	~25	-	66
	GA-MC	-	-	168*	-	67
	asMEG-O	-	-	174*	-	68
Carbon nanocage	CNCs	-	216	178	-	54
Carbon nanoscale network	CNN	195*	-	178*	-	69

*These gravimetric capacitances were measured under smaller current density provided in the headline.

Such a high power density meets the power requirement of the PNGV (Partnership for a New Generation of Vehicles) energy storage system performance goals,[71] and thus supports the applicability of UMCN-based supercapacitors as power supply components in hybrid vehicle systems.[63]

Conclusions

In conclusion, we demonstrate the development of novel UMCNs by the polymerization of R/F on the surfaces of P/T colloids in the presence of ammonia, followed by carbonization and further KOH activation. As-prepared UMCNs show tunable diameters (52–74 nm), high surface area (2156 m² g⁻¹) and unique core-shell ultramicroporous@microporous nanostructure. Nanosphere stacking mesopores, plentiful micropores coupled with regular ultramicropores facilitate ion transportation and diffusion and contribute to superb electrochemical performance. UMCNs as electrode materials for EDLCs exhibit a very high gravimetric capacitance of 411 F g⁻¹ at a current density of 1 A g⁻¹ in 6 M KOH electrolyte solution. Furthermore, the electrode shows ultra-high rate capability where an extremely large current density of 100 A g⁻¹ for charge–discharge operation is available. UMCNs also have superior electrochemical stability up to 10000 cycles at 10 A g⁻¹, and reasonable specific energy of 5.94 W h kg⁻¹ and high specific power density of 50 kW kg⁻¹ at 100 A g⁻¹. We believe that our methodology provide new opportunities for well-structured carbon nanoarchitectures to achieve advanced EDLCs for high rate electrochemical energy storage.

Notes and references

Shanghai Key Lab of Chemical Assessment and Sustainability, Department of Chemistry, Tongji University, 1239 Siping Road, Shanghai, 200092, P. R. China. Fax: 86 21 65981097; Tel: 86 21 65982654; E-mail: ganlh@tongji.edu.cn
† Electronic Supplementary Information (ESI) available. See DOI: 10.1039/b000000x/

1 L. L. Zhang and X. S. Zhao, *Chem. Soc. Rev.*, 2009, **38**, 2520–2531.

2 H. Jiang, P. S. Lee and C. Li, *Energy Environ. Sci.*, 2013, **6**, 41–53.

3 G. Q. Zhang, B. Y. Xia, C. Xiao, L. Yu, X. Wang, Y. Xie and X. W. Lou, *Angew. Chem. Int. Ed.*, 2013, **52**, 8643–8647.

4 J. Ye, W. Liu, J. Cai, S. Chen, X. Zhao, H. Zhou and L. Qi, *J. Am. Chem. Soc.*, 2011, 133, 933–940.

5 J. Zhu, M. Chen, N. Yerra, N.Haldolaarachchige, S. Pallavkar, Z. Luo, T. C Ho, J. Hopper, D. P. Young, S. Wei and Z. Guo, *Nanoscale*, 2013, **5**, 1825–1830.

6 M. Liu, X. Ma, L. Gan, Z. Xu, D. Zhu and L. Chen, *J. Mater. Chem. A*, 2014, **2**, 17107–17114.

7 J. Ren, L. Li, C. Chen, X. Chen, Z. Cai, L. Qiu, Y. Wang, X. Zhu and H. Peng, *Adv. Mater.*, 2013, **25**, 1155–1159.

8. J. L. Liu, L. L. Zhang, H. B. Wu, J. Y. Lin, Z. X. Shen and X. W. Lou, *Energy Environ. Sci.*, 2014, **7**, 3709–3719.

9. X. Ma, L. Gan, M. Liu, P. K. Tripathi, Y. Zhao, Z. Xu, D. Zhu and L. Chen. *J. Mater. Chem. A*, 2014, **2**, 8407–8415.

10. Z. Zhu, Y. Hu, H. Jiang and C. Li, *J. Power Sources*, 2014, **246**, 402–408.

11. S. Wang and R. A. W. Dryfe, *J. Mater. Chem. A*, 2013, **1**, 5279–5283.

12. S. Wang, B. Pei, X. Zhao and R. A.W. Dryfe, *Nano Energy*, 2013, **2**, 530–536.

13. J.-K. Chang, M.-T. Lee, W.-T. Tsai, M.-J. Deng, H.-F. Cheng and I.-W. Sun, *Langmuir*, 2009, **25**, 11955–11960.

14. M. Liu, L. Gan, W. Xiong, F. Zhao, X. Fan, D. Zhu, Z. Hao and L. Chen. *Energy Fuels*, 2013, **27**, 1168–1173.

15. P. Simon and Y. Gogotsi, *Nat. Mater.*, 2008, **7**, 845–854.

16. H. Itoi, H. Nishihara, T. Kogure and T. Kyotani, *J. Am. Chem. Soc.*, 2011, **133**, 1165−1167.

17. V. Ruiz, C. Blanco, R. Santamaría, J. M. Ramos-Fernández, M. Martínez-Escandell, A. Sepúlveda-Escribano and F. Rodríguez-Reinoso, *Carbon*, 2009, **47**, 195−200.

18. H.-J. Liu , J. Wang , C.-X. Wang and Y.-Y. Xia, *Adv. Energy Mater.*, 2011, **1**, 1101–1108.

19. L. Zhang, F. Zhang, X. Yang, K. Leng, Y. Huang and Y. Chen, *Small*, 2013, **9**, 1342−1347.

20. D. Zhu, Y. Wang, L. Gan, M. Liua, K. Cheng, Y. Zhao, X. Deng and D. Sun, *Electrochimica Acta*, 2015, **158**, 166−174.

21. L. Dai, D. W. Chang, J. B. Baek and W. Lu, *Small*, 2012, **8**, 1130−1166.

22. H. Jiang, J. Ma and C. Li, *Adv. Mater.*, 2012, **24**, 4197−4202.

23. W. Li, F. Zhang, Y. Dou, Z. Wu, H. Liu, X. Qian, D. Gu, Y. Xia, B. Tu and D. Zhao, *Adv. Energy Mater.*, 2011, **1**, 382–386.

24. B. Xu, S. Hou, H. Duan, G. Cao, M. Chu and Y. Yang, *J. Power Sources*, 2013, **228**, 193−197.

25. A. G. Pandolfo, and A. F. Hollenkamp, *J. Power Sources*, 2006, **157**, 11−27.

26. H. Nishihara, H. Itoi, T. Kogure, P. X. Hou, H. Touhara, F. Okino and T. Kyotani, *Chem. Eur. J.*, 2009, **15**, 5355−5363.

27. Y. Zhao, M. Liu, L. Gan, X. Ma, D. Zhu, Z. Xu and L. Chen, *Energy Fuels*, 2014, **28**, 1561−1568.

28. Y. Zhao, M. Liu, X. Deng, L. Miao, P. K. Tripathi, X. Ma, D. Zhu, Z. Xu, Z. Hao and L. Gan, *Electrochimica Acta*, 2015, **153**, 448–455.

29. J. Chmiola, G. Yushin, Y. Gogotsi, C. Portet, P. Simon and P. L. Taberna, *Science*, 2006, **313**, 1760−1763.

30. C. Largeot, C. Portet, J. Chmiola, P. L. Taberna, Y. Gogotsi and P. Simon, *J. Am. Chem. Soc.*, 2008, **130**, 2730−2731.

31. J. Chmiola, C. Largeot, P. L. Taberna, P. Simon and Y. Gogotsi, *Angew. Chem., Int. Ed.*, 2008, **47**, 3392−2295.

32. N. P. Wickramaratne, J. Xu, M. Wang, L. Zhu, L. Dai and M. Jaroniec, *Chem. Mater.*, 2014, **26**, 2820–2828.

33. W. Xiong, M. Liu, L. Gan, Y. Lv, Y. Li, L. Yang, Z. Xu, Z. Hao, H. Liu and L. Chen, *J. Power Sources*, 2011, **196**, 10461–10464.

34. C. X. Guo and C. M. Li, *Energy Environ. Sci.*, 2011, **4**, 4504–4507.

35. H. Dong, Z. Zhu, H. Ju and F. Yan, *Biosens. Bioelectron.*, 2012, **33**, 228–232.

36. J. Qian, M. Liu, L. Gan, P. K. Tripathi, D. Zhu, Z. Xu, Z. Hao, L Chen and D. S. Wright, *Chem. Commun.*, 2013, **49**, 3043–3045.

37. D.-D. Zhou, H.-J. Liu, Y.-G. Wang, C.-X. Wang and Y.-Y. Xia, *J. Mater. Chem.*, 2012, **22**, 1937–1943.

38. M. Liu, L. Gan, W. Xiong, Z. Xu, D. Zhu and L. Chen, *J. Mater. Chem. A*, 2014, **2**, 2555–2562.

39. Y. Fan, P.-F. Liu, Z.-Y. Huang, T.-W. Jiang, K.-L. Yao and R. Han, *J. Power Sources*, 2015, **280**, 30–38.

40. J. Liu, S. Z. Qiao, H. Liu, J. Chen, A. Orpe, D. Zhao and G. Q. Max Lu, *Angew. Chem., Int. Ed.*, 2011, **50**, 5947–5951.

41. J. Choma, D. Jamioła, K. Augustynek, M. Marszewski, M. Gao and M. Jaroniec, *J. Mater. Chem.*, 2012, **22**, 12636–12642.

42. S. Wang, W. Li, G. Hao, Y. Hao, Q. Sun, X. Zhang and A. Lu, *J. Am. Chem. Soc.*, 2011, **133**, 15304–15307.

43. D. Li, L. Ding, H. Chen, S. Wang, Z. Li, M. Zhu and H. Wang, *J. Mater. Chem. A*, 2014, **2**, 16617–16622.

44. J. Han, G. Xu, B. Ding, J. Pan, H. Dou and D. R. MacFarlane, *J. Mater. Chem. A*, 2014, **2**, 5352–5357.

45. Y. Fang, D. Gu, Y. Zou, Z. Wu, F. Li, R. Che, Y. Deng, B. Tu and D. Zhao, *Angew. Chem. Int. Ed.*, 2010, **49**, 7987–7991.

46. Z. Lei, N. Christov, L. L. Zhang and X. S. Zhao, *J. Mater. Chem.*, 2011, **21**, 2274–2281.

47. A. P. Katsoulidis and M. G. Kanatzidis, *Chem. Mater.*, 2011, **23**, 1818–1824.

48. A. P. Katsoulidis and M. G. Kanatzidis, *Chem. Mater.*, 2012, **24**, 471–479.

49. C. Liang and S. Dai, *J. Am. Chem. Soc.*, 2006, **128**, 5316–5317.

50. P. K. Tripathi, M. Liu, Y. Zhao, X. Ma, L. Gan, O. Noonan and C. Yu, *J. Mater. Chem. A*, 2014, **2**, 8534–8544.

51. K. S. W. Sing, D. H. Everett, R. A. W. Haul, L. Moscou, R. A. Pierotti, J. Rouquérol and T. Siemieniewska, *Pure Appl. Chem.*, 1985, **57**, 603−619.

52. W. Gao, Y. Wan, Y. Dou and D. Zhao, *Adv. Energy Mater.*, 2011, **1**, 115−123.

53. L. Yang, S. Cheng, Y. Ding, X. Zhu, Z. L. Wang and M. Liu, *Nano Lett.*, 2011, 12, 321−325.

54. K. Xie, X. Qin, X. Wang, Y. Wang, H. Tao, Q. Wu, L.Yang and Z. Hu, *Adv. Mater.*, 2012, **24**, 347−352.

55. C. Merlet, B. Rotenberg, P. A. Madden, P. Taberna, P. Simon, Y. Gogotsi and M. Salanne, *Nat. Mater.*, 2012, **11**, 306−310.

56. M. Salari, K. Konstantinov and H. K. Liu, *J. Mater. Chem.*, 2011, **21**, 5128–5133.

57. B. Liu, H. Shioyama, H. Jiang, X. Zhang and Q. Xu, *Carbon*, 2010, **48**, 456−463.

58. H.-L. Jiang, B. Liu, Y.-Q. Lan, K. Kuratani, T. Akita, H. Shioyama, F. Zong and Q. Xu, *J. Am. Chem. Soc.*, 2011, **133**, 11854–11857.

59. Y. Lv, F.Zhang, Y. Dou, Y. Zhai, J. Wang, H. Liu, Y. Xia, B. Tu and D. Zhao, *J. Mater. Chem.*, 2012, **22**, 93−99.

60. D. Feng, Y. Lv, Z. Wu, Y. Dou, L. Han, Z. Sun, Y. Xia, G. Zheng and D. Zhao, *J. Am. Chem. Soc.*, 2011, **133**, 15148–15156.

61. Q. Li, R. Jiang, Y. Dou, Z. Wu, T. Huang, D. Feng, J. Yang, A. Yu and D. Zhao, *Carbon*, 2011, **49**, 1248−1257.

62. Y. Lv, L. Gan, M. Liu, W. Xiong, Z. Xu, D. Zhu and D. S. Wright, *J. Power Sources*, 2012, **209**,152−157.

63. D. Wang, F. Li, M. Liu, G. Q. Lu and H. Cheng, *Angew. Chem. Int. Ed.*, 2008, 47, 373−376.

64. D.-Y. Kang and J. H. Moon, *ACS Appl. Mater. Interfaces*, 2014, **6**, 706–711.

65. Q. Wang, J. Yan, Y. Wang, G. Ning, Z. Fan, T. Wei, J. Cheng, M. Zhang and X. Jing, *Carbon*, 2013, **52**, 209–218.

66. Y. R. Kang, Y. L. Li, F. Hou, Y. Y. Wen and D. Su, *Nanoscale*, 2012, **4**, 3248–3253.

67. Z.-S. Wu, Y. Sun, Y.-Z. Tan, S. Yang, X. Feng and K. Müllen, *J. Am. Chem. Soc.*, 2012, **134**, 19532−19535.

68. T.Y. Kim, G. Jung, S. Yoo, K. S. Suh and R. S. Ruoff, *ACS Nano*, 2013, **7**, 6899–6905.

69. Z. Li, D. Wu, X. Huang, J. Ma, H. Liu, Y. Liang, R. Fu and K. Matyjaszewski, *Energy Environ. Sci.*, 2014, **7**, 3006–3012.

70. S. Y. Kim, H. M. Jeong, J. H. Kwon, W. Ock, W. H. Suh, G. D. Stucky and J. K. Kang, *Energy Environ. Sci.*, 2015, **8**, 188–194.

71. R. F. Nelson, *J. Power Sources*, 2000, **91**, 2–26.

Graphical Abstract

Core-shell ultramicroporous@microporous carbon nanospheres as advanced supercapacitor electrodes

Mingxian Liu, Jiasheng Qian, Yunhui Zhao, Dazhang Zhu, Lihua Gan* and Longwu Chen

Core-shell ultramicroporous@microporous carbon nanospheres were developed as advanced supercapacitor electrodes for high rate electrochemical energy storage.

1